materials

MDPI

Article

Acacia nilotica Pods' Extract Assisted-Hydrothermal Synthesis and Characterization of ZnO-CuO Nanocomposites

Manal Hessien [1,*], Amel Taha [1,2] and Enshirah Da'na [3]

[1] Department of Chemistry, College of Science, King Faisal University, P.O. Box 400, Al-Ahsa 31982, Saudi Arabia; ataha@kfu.edu.sa
[2] Department of Chemistry, Faculty of Science and Technology, Al-Neelain University, Khartoum 11121, Sudan
[3] Department of Biomedical Engineering, Faculty of Engineering, King Faisal University, P.O. Box 400, Al-Ahsa 31982, Saudi Arabia; edana@kfu.edu.sa
* Correspondence: mhessien@kfu.edu.sa

Abstract: This work represents a novel combination between *Acacia nilotica* pods' extract and the hydrothermal method to prepare nanoparticles of pure zinc oxide and pure copper oxide and nanocomposites of both oxides in different ratios. Five samples were prepared with different ratios of zinc oxide and copper oxide; 100% ZnO (ZC0), 75% ZnO: 25% CuO (ZC25), 50% ZnO: 50% CuO (ZC50), 25% ZnO: 75% CuO (ZC75), and 100% CuO (ZC100). Several techniques have been applied to characterize the prepared powders as FTIR, XRD, SEM, and TEM. The XRD results confirm the formation of the hexagonal wurtzite phase of zinc oxide and the monoclinic tenorite phase of copper oxide. The microscopy results show the formation of a heterostructure of nanocomposites with an average particle size of 13–27 nm.

Keywords: *Acacia nilotica*; wurtzite ZnO; tenorite CuO; nanocomposite; microstructure

Citation: Hessien, M.; Taha, A.; Da'na, E. *Acacia nilotica* Pods' Extract Assisted-Hydrothermal Synthesis and Characterization of ZnO-CuO Nanocomposites. *Materials* **2022**, *15*, 2291. https://doi.org/10.3390/ma15062291

Academic Editor: Ana Pimentel

Received: 23 February 2022
Accepted: 18 March 2022
Published: 20 March 2022

1. Introduction

Zinc oxide has been widely applied as photocatalysts [1–4], antimicrobial agents [5–7], supercapacitors [8,9], sensors [6,10], varistor [11], biosensors [10], in solar cells [12–14], transparent electrodes [15], and fuel cells [9,16]. This wide range of applications is based on the characteristics of ZnO as an n-type semiconductor, low-cost, chemical, and thermal stability, a direct band gap (~3.3 eV), and binding energy of 60 meV [17,18]. Despite all these characteristics, there are two limitations to commercializing zinc oxide applications. First, its light absorption falls in the UV region, which deprived zinc oxide of the visible light absorption. Second, its high rate of charge recombination collapses its photocatalytic activity. To overcome these drawbacks, a doping zinc oxide or forming composite is applied [6].

Q. Zeng et al. reported enhanced gas sensing properties of NiO-ZnO nanocomposites, which they attributed to the formation of a p-n heterojunction [19]. The same observation was reported by the Yang group regarding the fast response of the Co_3O_4-ZnO gas sensor towards triethylamine [20]. Y. Wang et al. successfully enhanced the absorption of zinc oxide to be in the visible region through forming ZnO-MnO with a bandgap = 2.2 eV with Mn^{2+} = 50 at.% [21]. M. Toe et al. tuned the bandgap of ZnO through compositing it with CuO, NiO, and Al_2O_3, which changed the bandgap to 3.17 eV, 3.28 eV and 3.16 eV, respectively [22]. Copper oxide is a p-type semiconductor with a bandgap in the range of 1.2–2 eV. CuO is characterized by a low-cost and non-toxic material which makes it a good component to form a composite with ZnO.

Various methods are applied to prepare metal oxide nanoparticles and nanocomposites as simple precipitation [23], electrochemical method [24], mechanical milling [1], sol-gel method [2,25], biocombustion [26], co-precipitation [27], green synthesis [28,29], sonochemical synthesis [30] and hydrothermal method [31,32]. The hydrothermal method

has many advantages as being simple, low-cost, and low-temperature. Green synthesis involves the use of plant extracts as capping agents and/or reducing agents instead of using synthetic surface directing agents as surfactants or polymers which may harm the environment [18,33,34].

R. Mohamed et al. prepared CuO-ZnO heterojunction photocatalyst through a simple wet method in the presence of F-127 surfactant [35]. A. Prajapati et al. prepared CuO-ZnO-C nanocomposites by using extract of *Tagetes* spp. petals in the presence of CTAB surfactant [36]. Moreover, the vapor deposition technique was used to prepare CuO-ZnO and applied in optoelectronics [37]. ZnO-CuO has been prepared by green synthesis using *Sambucus nigra* L. extract [28].

Acacia nilotica, also known as gum arabic tree, belongs to the *Fabaceae* family. It is popular in Africa and Asia and the tree has roots, pods, stems, and leaves. The extract has many phytochemical components as flavonoids, phenols, and tannins [38,39]. The pods have been applied in the synthesis of copper oxide nanoparticles [40], the leaves have been used in the preparation of silver nanoparticles [38], the aerial parts of *Acacia nilotica* have been used to prepare Ag-TiO_2 nanocomposites [41].

The recent work reports for the first time the combination between a green synthesis that employs *Acacia nilotica* Pods' extract and the hydrothermal method. Pristine zinc oxide and copper oxide nanoparticles were synthesized in addition to copper oxide-zinc oxide nanocomposites with different ratios. The functional groups and the formed phases were determined by Fourier Transform Infrared spectroscopy (FTIR) and X-ray diffraction (XRD), respectively. The morphology and particle size were followed by scanning electron microscopy (SEM) and transmission electron microscopy (TEM).

2. Materials and Methods

2.1. Materials and Instruments

Copper chloride hexahydrate ($CuCl_2.6H_2O$), zinc chloride ($ZnCl_2$), potassium hydroxide (KOH) were bought from Sigma-Aldrich. All the primary chemicals used in this work were of analytical grade. All solutions were prepared with double-distilled water. The *Acacia nilotica* pods were bought from a local store, Al-Ahsa, Saudi Arabia.

The FTIR analysis of the copper oxide and zinc oxide nanoparticles and nanocomposites was analyzed on Cary 630 FT-IR spectrophotometer. The XRD analysis was performed on Bruker D8 X-ray Diffractometer with Ni-filtered Cu-Kα radiation and a graphite monochromator to produce X-rays with a wavelength of 1.5418 Å at 35 kV and 25 mA, using glancing-angle from 10° to 60° at scan steps of 0.02° with an accuracy $\leq$ 0.001°. For further surface morphology, Scanning Electron Microscope (SEM) (Philips XL30) was used, accelerating voltage of 30 kV and the magnification up to 400,000×. A high-resolution, JEOL JEM-1011 Transmission Electron Microscope was used for TEM imaging.

2.2. Acacia nilotica Extraction

The *Acacia nilotica* pods were rinsed with tap water three times and with distilled water for the last time. To prepare the extract, 10 g of dried pods were boiled with 100 mL of distilled water at 60 °C for 15 min under magnetic stirring. The prepared extract was centrifuged at 8000 rpm for 5 min and then filtered via Whatman No. 1 filter paper, to remove all fine plant debris and stored at 4 °C [42]. The pH of the extract is 5.71.

2.3. Green Synthesis

A 0.2 M solution of copper chloride hexahydrate ($CuCl_2.6H_2O$) and a 0.2 M solution of zinc chloride ($ZnCl_2$) were prepared in two different containers. The compositions of samples are mentioned in Table 1. As an example, 20 mL of the *Acacia nilotica* extract is added to a 100 mL of 0.2 M zinc chloride salt solution to prepare sample ZC0. A 1 M KOH was added to the previous mixture while under continuous stirring until the pH reaches 10.

Table 1. Sample codes and corresponding volumes of precursors (mL).

Sample Code	ZC0	ZC25	ZC50	ZC75	ZC100
$ZnCl_2$	100	75	50	25	0
$CuCl_2.6H_2O$	-	25	50	75	100

2.4. Hydrothermal Synthesis

The prepared precipitate was transferred to a Teflon-lined autoclave, which was placed in an oven at 250 °C for 2.5 h. After the completion of hydrothermal treatment, the solution is subjected to sonication for an hour in 100 mL distilled water. The sample was then left to settle down and the liquor was disposed of. The sonication and settling down steps were repeated three times with water and one time with ethanol. The sonication was executed by using Power sonic405 ultrasonic bath to cleanse the samples. The samples were dried in an oven overnight at 75 °C. In the end, the samples were calcined at 300 °C for 2 h to get rid of the extract residuals. Scheme 1 represents the synthesis steps.

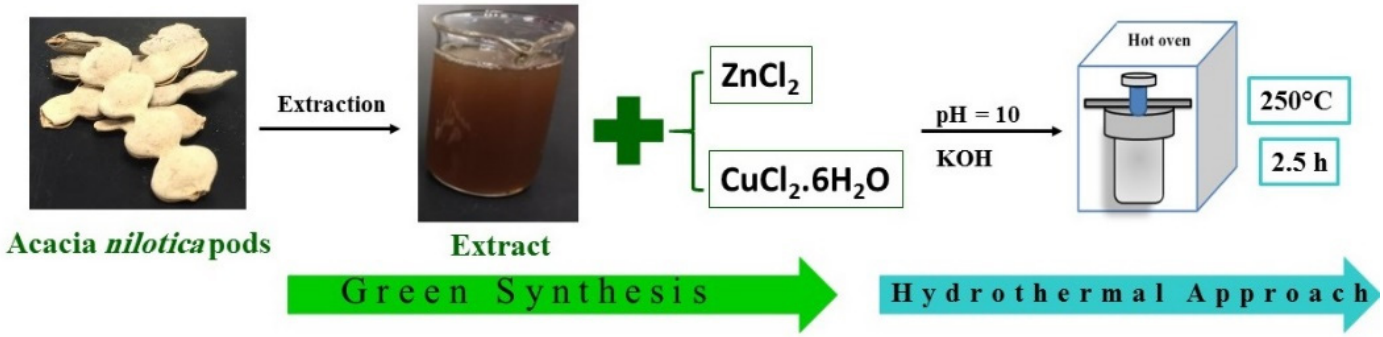

Scheme 1. The synthesis steps for samples prepared by green assisted-hydrothermal method.

3. Results

3.1. FTIR Characterization

Figure 1 represents the FTIR of ZC0, ZC25, ZC50, ZC75 and ZC100 samples after calcination at 300 °C for 2 h. In some samples, a shallow broad peak around 3200 cm^{-1} is assigned for the OH group. The peak at 1600 cm^{-1} is assigned for absorbed water molecules from the surrounding [43]. The peaks below 700 cm^{-1} can be assigned to metal–oxygen bonds in both zinc oxide and copper oxide [44]. In sample ZC0, which is pristine zinc oxide, the deep peak below 700 cm^{-1} is assigned for the Zn-O bond [32]. The depth of this peak decreases as the content of ZnO decreases in samples ZC25, ZC50 and ZC75, respectively. In sample ZC100, which is pristine copper oxide, the less deep peak below 600 cm^{-1} indicates the presence of Cu-O. Going from sample ZC75, ZC50 to ZC25, the depth of this band increases as the content of copper oxide decreases and the content of zinc oxide increases [26]. The FTIR results confirm the formation of pristine zinc oxide, zinc oxide-copper oxide nanocomposites and pristine copper oxide in samples ZC0, ZC25, ZC50, ZC75, and ZC100, respectively.

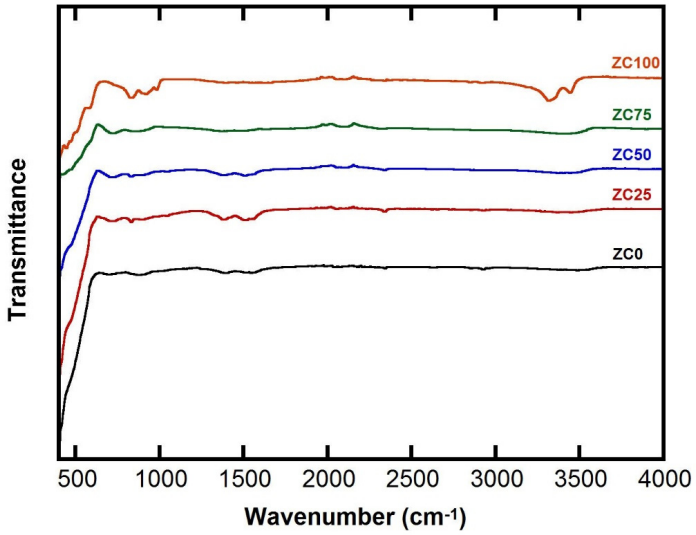

Figure 1. FTIR spectra of the ZC0, ZC25, ZC50, ZC75, and ZC100 samples.

Figure 2a represents the FTIR of *Acacia nilotica* pods' extract, sample ZC50 (b) after precipitation, (c) after hydrothermal treatment and drying and (d) after calcination. The FTIR of *Acacia nilotica* pods' extract shows a very broad band between 2800–3600 cm^{-1} which may correspond to the stretching vibration of aromatic and aliphatic OH groups (3200–3500 cm^{-1}) or stretching of aromatic and aliphatic C-H (3000–3100 cm^{-1}). A sharp finger-like peak around 1500–1700 cm^{-1} stands for carbonyl groups or bending of aromatic C=C. A very broad band below 1000 cm^{-1} may refer to the bending of aromatic C-H or C-O-C groups. According to the literature, the FTIR results of *Acacia nilotica* pods' extract confirm the presence of flavonoids, tannins and terpenoids in the extract [38,39]. The FTIR spectrum of sample ZC50 after adding KOH is shown in Figure 2b where all the peaks of the extract can be seen. Figure 2c shows the FTIR spectrum of the sample after the hydrothermal treatment and drying which results in the disappearance of the peaks related to the extract. Figure 2d shows the FTIR of the sample after calcination at 300 °C for 2 h, which results in the sharpness of peaks related to M-O bonds between 400–600 cm^{-1} [26].

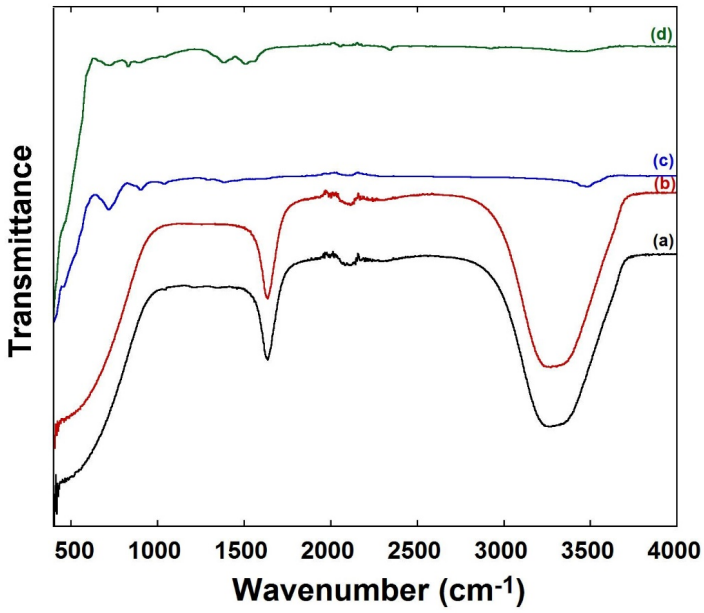

Figure 2. The FTIR spectra of (**a**) Acacia extract. (**b**) Sample ZC50 after precipitation. (**c**) Sample ZC50 after hydrothermal treatment and drying. (**d**) Sample ZC50 after calcination.

3.2. XRD Characterization

Figure 3 represents the XRD patterns of the samples ZC0, ZC25, ZC50, ZC75, and ZC100 prepared by the green-hydrothermal technique (pH = 10, T = 250 ∘C, t = 2.5 h) and calcined at 300 °C for 2 h. The ZC0 sample shows peaks at 2θ~31.96°, 34.61°, 36.44°, 47.74°, and 56.73° corresponding to the diffraction planes (1 0 0), (0 0 2), (1 0 1), (0 1 2), and (1 1 0) of a wurtzite hexagonal structure according to Card no. 96-900-4179 [36]. The XRD results confirm that sample ZC0 is formed completely of zincite, which is pure zinc oxide with a hexagonal phase. For the sample ZC100, the peaks appear at 2θ~32.47°, 35.60°, 38.90°, 48.96°, and 53.576° for (1 1 0), (11-1), (1 1 1), (2 0-2), and (0 2 0) according to Card no. 96-721-2243, which represents the monoclinic phase of copper oxide. The XRD results confirm that sample ZC100 is formed completely of tenorite, which is pure copper oxide with a monoclinic phase [36,45–47].

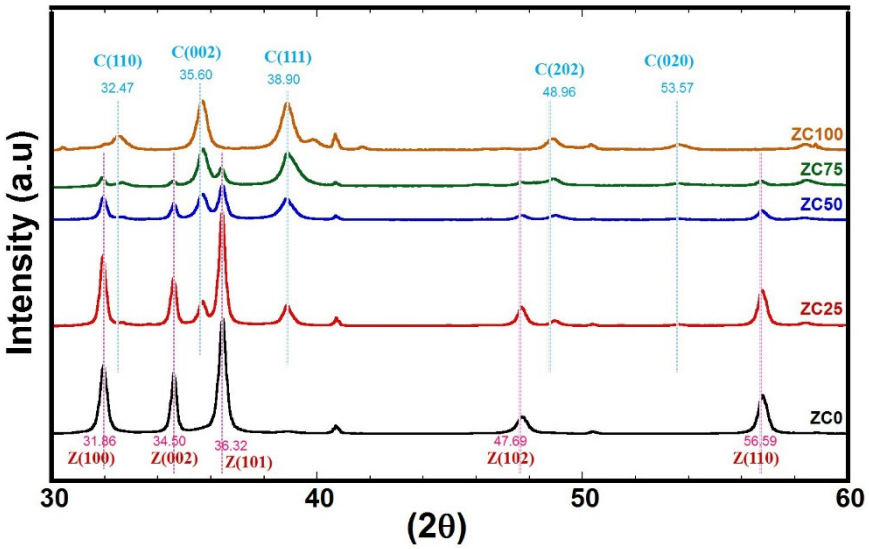

Figure 3. The XRD patterns of the ZC0, ZC25, ZC50, ZC75, and ZC100 samples.

Samples ZC25, ZC50, and ZC75 show the peaks corresponding to wurtzite hexagonal zinc oxide and tenorite monoclinic copper oxide with different intensities. However, the intensity of peaks corresponding to wurtzite zinc oxide is decreasing gradually in the samples ZC25, ZC50, and ZC75 with decreasing the amount of zinc precursor in the starting materials. The same can be observed in an opposite way for the monoclinic tenorite and the intensity of copper oxide peaks increases gradually in samples ZC25, ZC50, ZC75 with an increasing copper precursor in the initial compositions (Table 1) [2,26,48]. There are no peaks detected by XRD for Zn metal, Cu metal, or any other compounds which indicates the high purity of formed ZnO-CuO nanocomposites. In addition, there is no observed shift in the corresponding peaks of either ZnO or CuO, which indicates the heterostructure formation of ZnO-CuO and no incorporation [49].

The crystallite size of zinc oxide and copper oxide is estimated using the Debye–Scherrer formula and presented in Figure 4 [50]. The crystallite size of zinc oxide is calculated based on the main peak corresponding to plane (101) and based on the main peak corresponding to plane (111) of tenorite copper oxide. The crystallite size of pristine zinc oxide is 26 nm, and the crystallite size of pristine copper oxide is 29 nm. It seems that adding copper oxide (25%) to zinc oxide derives a rise in the crystallite size of zinc oxide to 30 nm compared to pristine zinc oxide (26 nm). Further increase of copper oxide (50% and 75%) develops a decrease in the crystallite size of zinc oxide to 21 nm and 17 nm, respectively. On the other hand, adding zinc oxide to copper oxide produces a decrease in the crystallite size of copper oxide to 15 nm, 21 nm, and 27 nm in samples (ZC 75, ZC50, and ZC25) compared to 29 nm of pristine copper oxide. A. Lavin et al. prepared ZnO-CuO nanocomposites through the sol-gel method and found that the crystallite size of zinc oxide and copper

oxide varied with composition [47]. It is worth noting that in their results when a sample has equal amounts of zinc oxide and copper oxide; the crystallite size is about 48 nm for both oxides. In another study, the average crystallite size of ZnO/CuO nanocomposite powders was 30 nm when the solvent was water and it decreased to 25 nm when the solvent changed to water/ethanol [44]. While in this work, sample ZC50 has a crystallite size of 21 nm for both oxides. This may be related to the effect of capping agents found in *Acacia nilotica* extract, which seems to be more effective as a capping agent than ethanol as a solvent in decreasing the crystallite size [47]. C. Kumar et al. prepared ZnO-CuO by combustion method assisted with extract of *Calotropis gigantea*, and the average crystallite size was about 35 nm [29]. M. Mansourina et al. reported that the average crystallite size of hydrothermally synthesized ZnO and CuO are 26 and 21 nm, respectively. It is worth noting that the mentioned crystallite size is for the as-prepared samples, which are smaller than the crystallite size of the calcined samples [51]. Again, the integration of hydrothermal with green synthesis resulted in a less average crystallite size. Ultimately, the XRD results show that the green assisted-hydrothermal method successfully synthesizes zinc oxide nanoparticles, copper oxide nanoparticles, and zinc oxide–copper oxide nanocomposites with no other alloys or intermediate compounds with crystallite size 15–29 nm.

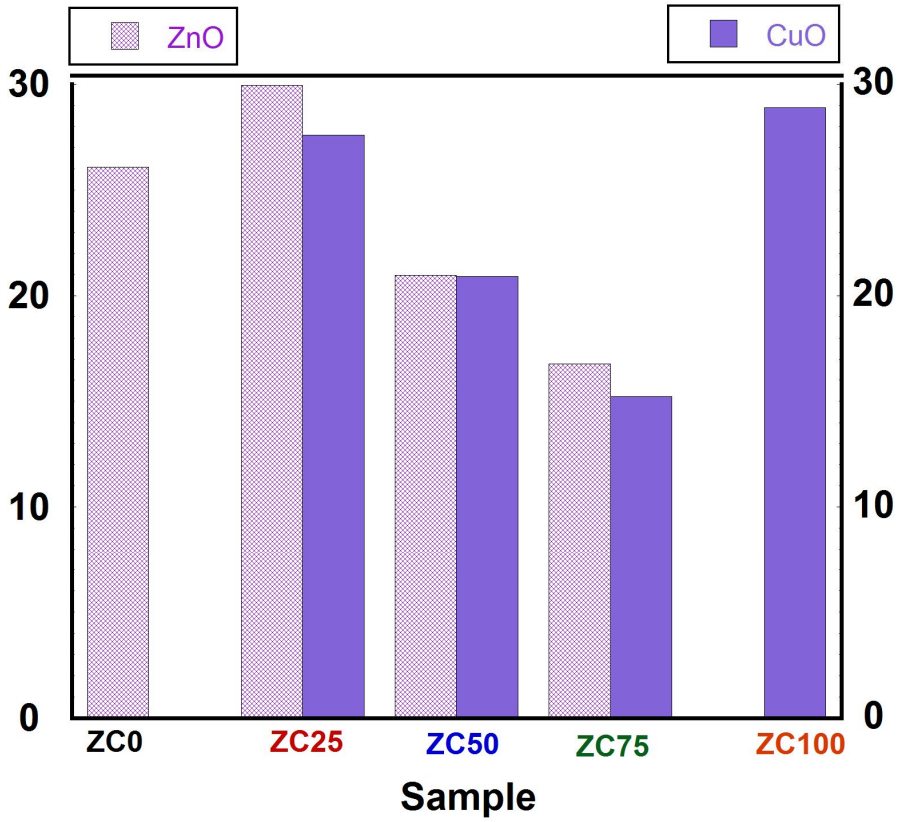

Figure 4. The crystallite size as calculated by Scherrer's Equation of the ZC0, ZC25, ZC50, ZC75, and ZC100 samples.

3.3. Morphology

Figure 5 represents the surface morphology of the different samples as investigated by SEM. Sample ZC0 is shown in Figure 5a,b and its morphology is composed of agglomerated particles along with stacked layers. In our previous work on hydrothermally prepared pristine ZnO without capping agents, ZnO had a morphology of short nanorods or nanoflakes depending on the synthesis conditions [52]. Sample ZC100 is presented in Figure 5i,j and it is formed of bipyramidal morphology. M. Quirino et al. prepared CuO with a microwave hydrothermal method without any surfactants, and it resulted in a plate-like shape [53].

P. Gao et al. prepared CuO with a hydrothermal method without any surfactants, and it resulted in a dumbbell-like morphology [54]. H. Chen et al. prepared CuO with a hydrothermal method in the presence of sodium dodecyl benzenesulfonate as a soft template, which resulted in the formation of 3D nanobundles consisted of nanorods [55]. *Acacia nilotica* phytoexctract acted as capping agents which enhances the growth of CuO bipyramid.

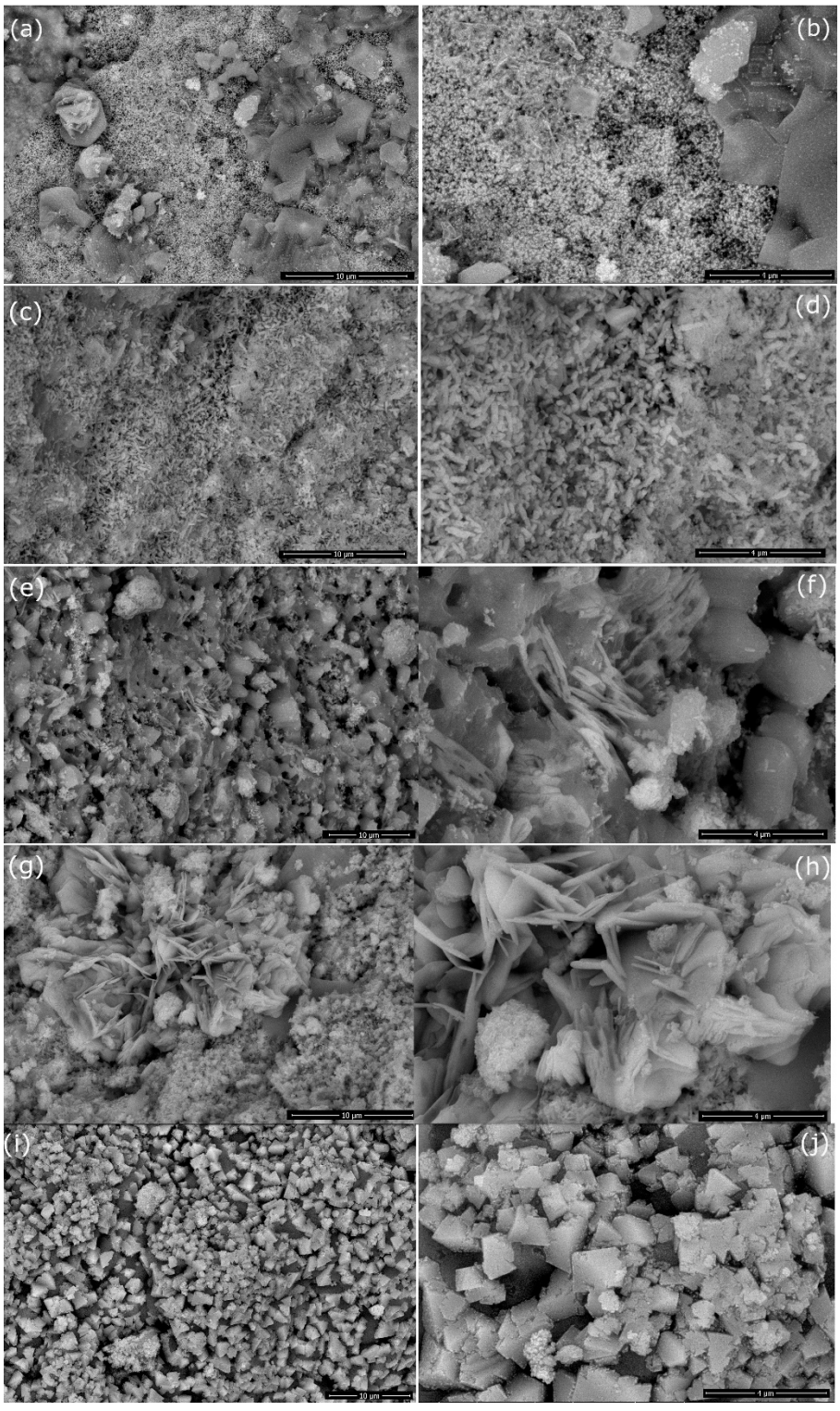

Figure 5. The SEM photos of the ZC0 (**a**,**b**), ZC25 (**c**,**d**), ZC50 (**e**,**f**), ZC75 (**g**,**h**), and ZC100 (**i**,**j**) samples.

Adding 25% copper oxide into zinc oxide resulted in changing the morphology from stacked layers/aggolmerated particles into homogenous elongated particles, as can be depicted in Figure 5c,d. Increasing copper oxide to 50% resulted in intermeshed flakes of ZnO along with CuO particles, Figure 5e,f. In sample ZC75, Figure 5g,h, the zinc oxide is represented by rosette shape and copper oxide has a smaller particle size compared to sample ZC50. H. Ullah et al. prepared ZnO-CuO nanocomposites with vegetable waste extract of cauliflowers, potatoes, and peas, and they found that the extract type has an impact on the morphology. The morphology of ZnO-CuO prepared with cauliflowers, potatoes, and peas were rods, a mixture of rods/spindles, and nanoparticles, respectively [56]. V. Kumari et al. prepared ZnO-CuO with a hydrothermal synthesis without any surfactants with a Zn/Cu molar ratio = 8:1, which resulted in a bittergourd morphology [57]. M. Mansournia et al. reported that CuO did not form individual morphology of CuO when CuO = 0.4, 2 and 10% CuO. However, CuO nanoplates were formed when the CuO increased to 50% along with ZnO-CuO nanoparticles [51]. P. Lu et al. prepared CuO-ZnO nanocomposites via hydrothermal method and reported that pristine CuO and pristine ZnO have nanosheets that collapsed into smaller sheets with increasing CuO [58]. T. Chang et al. prepared CuO-ZnO nanocomposites via hydrothermal method and reported that the morphology of pristine ZnO is nanoplates and the morphology of CuO in ZnO-CuO nanocomposites is nanoparticles well-distributed with ZnO [59].

Figure 6 represents the TEM photos for the samples after calcination. The SAED images of all the samples approve the formation of crystalline materials, which is reflected through concentric rings which have been discussed in the XRD results. The average particle size drawn from TEM is about 13 nm, 14 nm, 15 nm, 26 nm, and 27 nm for samples ZC0, ZC25, ZC50, ZC75, and ZC100, respectively. Figure 6a,b represents sample ZC0 and its images show spherical particles and polygonal shapes. Figure 6c,d, sample ZC25, shows a ZnO elongated shape on the bottom left corner with small spherical particles on its surface, which may be referred to as CuO. Sample ZC50, in Figure 6e,f, and Sample ZC75, in Figure 6g,h, show spherical particles of CuO along with flake of ZnO, which highlights the efficiency of the extract in heterojunction formation [60]. The same observation was reported by J. Singh et al., who prepared CuO decorated ZnO nanoflakes by a hydrothermal method assisted with cetyltetra amine bromide (CTAB). Sample ZC100 shows spherical particles of CuO, as shown in Figure 6. The TEM results are in agreement with SEM results.

In the present study, ZnO NPs, ZnO-CuO NCs, and CuO NPs have been prepared by an inexpensive and environmentally friendly method; the green-hydrothermal method. The proposed mechanism is presented in the following equations;

$$CuCl_2.6H_2O\ (aq) + 2KOH + \text{phytoconstituents of extract} \rightarrow Cu(OH)_2 \text{ capped with phytoconstituents} + 2KCl$$

$$ZnCl_2\ (aq) + 2KOH + \text{phytoconstituents of extract} \rightarrow Zn(OH)_2 \text{ capped with phytoconstituents} + 2KCl$$

$$Cu(OH)_2/Zn(OH)_2\ (\text{hydrothermal treatment}) \rightarrow CuO/ZnO$$

The presence of phytoconstituents, i.e., flavonoids, tannins, and terpenoids; in the *Acacia nilotica* pods' extract act as capping agents. The capping agents play an important role in decreasing the agglomeration and in controlling the growth during the hydrothermal step.

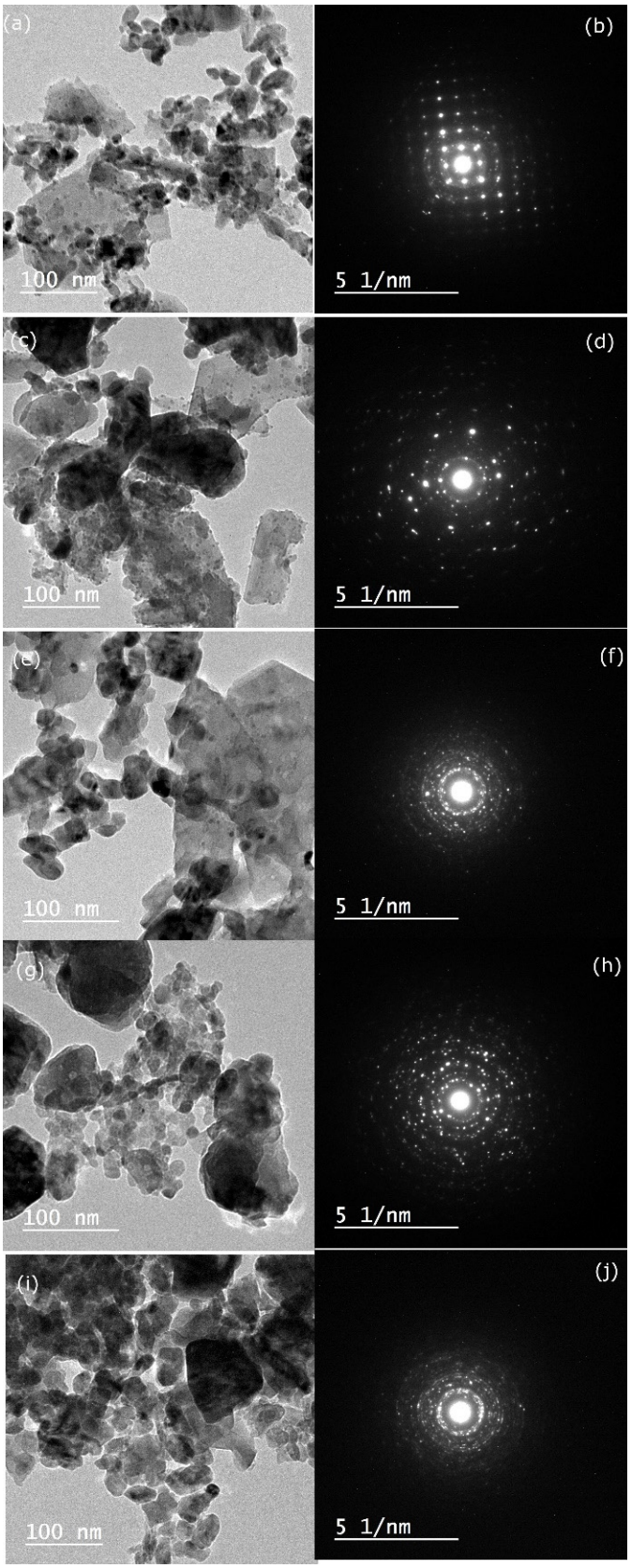

Figure 6. The TEM photos of ZC0 (**a**,**b**), ZC25 (**c**,**d**), ZC50 (**e**,**f**), ZC75 (**g**,**h**), and ZC100 (**i**,**j**) samples.

4. Conclusions

In the recent work, successful combination of *Acacia nilotica* pods' extract with the hydrothermal method resulted in the synthesis of ZnO NPs, ZnO-CuO NCs, and CuO NPs. The prepared ZnO NPs have a hexagonal wurtzite phase and the CuO NPs have a monoclinic tenorite phase. Interestingly, ZnO-CuO NCs have a hexagonal phase for ZnO and a monoclinic phase for CuO with no secondary phases. The average crystallite size of NPs and NCs is in the range of 17–30 nm. The morphology of the particles depend on the ratio ZnO-CuO and the prepared particles showed different morphologies as agglomerated particles, nanorods, intermeshed flakes together with irregularly shaped particles.

Author Contributions: Conceptualization, M.H.; methodology, M.H. and A.T.; formal analysis, M.H.; investigation, M.H., A.T. and E.D.; resources, M.H. and A.T.; data curation, M.H.; writing—original draft preparation, M.H.; writing—review and editing, M.H. and E.D.; visualization, M.H.; project administration, M.H.; funding acquisition, M.H. All authors have read and agreed to the published version of the manuscript.

Funding: This research was funded by the Deanship of Scientific Research, King Faisal University, Saudi Arabia, grant number NA000245 and the APC was funded by Deanship of Scientific Research at King Faisal University.

Institutional Review Board Statement: Not applicable.

Informed Consent Statement: Not applicable.

Data Availability Statement: Data only available upon request from the corresponding author.

Conflicts of Interest: The authors declare no conflict of interest.

References

1. Yarahmadi, M.; Maleki-Ghaleh, H.; Mehr, M.E.; Dargahi, Z.; Rasouli, F.; Siadati, M.H. Synthesis and characterization of Sr-doped ZnO nanoparticles for photocatalytic applications. *J. Alloys Compd.* **2021**, *853*, 157000. [CrossRef]
2. Truong, T.T.; Pham, T.T.; Truong, T.T.T.; Pham, T.D. Synthesis, characterization of novel ZnO/CuO nanoparticles, and the applications in photocatalytic performance for rhodamine B dye degradation. *Environ. Sci. Pollut. Res. Int.* **2021**, *29*, 22576–22588. [CrossRef] [PubMed]
3. Azar, B.E.; Ramazani, A.; Fardood, S.T.; Morsali, A. Green synthesis and characterization of $ZnAl_2O_4$@ZnO nanocomposite and its environmental applications in rapid dye degradation. *Optik* **2020**, *208*, 164129. [CrossRef]
4. Náfrádi, M.; Alapi, T.; Farkas, L.; Bencsik, G.; Kozma, G.; Hernádi, K. Wavelength Dependence of the Transformation Mechanism of Sulfonamides Using Different LED Light Sources and TiO_2 and ZnO Photocatalysts. *Materials* **2021**, *15*, 49. [CrossRef] [PubMed]
5. Kumar, C.R.R.; Betageri, V.S.; Nagaraju, G.; Pujar, G.H.; Onkarappa, H.S.; Latha, M.S. Synthesis of Core/Shell (ZnO/Ag) Nanoparticles Using *Calotropis gigantea* and Their Applications in Photocatalytic and Antibacterial Studies. *J. Inorg. Organomet. Polym. Mater.* **2020**, *30*, 3410–3417. [CrossRef]
6. Wang, J.; Chen, R.; Xiang, L.; Komarneni, S. Synthesis, properties and applications of ZnO nanomaterials with oxygen vacancies: A review. *Ceram. Int.* **2018**, *44*, 7357–7377. [CrossRef]
7. Achouri, F.; Merlin, C.; Corbel, S.; Alem, H.; Mathieu, L.; Balan, L.; Medjahdi, G.; Ben Said, M.; Ghrabi, A.; Schneider, R. ZnO Nanorods with High Photocatalytic and Antibacterial Activity under Solar Light Irradiation. *Materials* **2018**, *11*, 2158. [CrossRef] [PubMed]
8. Murali, S.; Dammala, P.K.; Rani, B.; Santhosh, R.; Jadhao, C.; Sahu, N.K. Polyol mediated synthesis of anisotropic ZnO nanomaterials and composite with rGO: Application towards hybrid supercapacitor. *J. Alloys Compd.* **2020**, *844*, 156149. [CrossRef]
9. Ponnamma, D.; Cabibihan, J.-J.; Rajan, M.; Pethaiah, S.S.; Deshmukh, K.; Gogoi, J.P.; Pasha, S.K.K.; Ahamed, M.B.; Krishnegowda, J.; Chandrashekar, B.N.; et al. Synthesis, optimization and applications of ZnO/polymer nanocomposites. *Mater. Sci. Eng. C* **2019**, *98*, 1210–1240. [CrossRef] [PubMed]
10. Shetti, N.P.; Bukkitgar, S.D.; Reddy, K.R.; Reddy, C.V.; Aminabhavi, T.M. ZnO-based nanostructured electrodes for electrochemical sensors and biosensors in biomedical applications. *Biosens. Bioelectron.* **2019**, *141*, 111417. [CrossRef] [PubMed]
11. Xie, P.; Wang, Z.; Wu, K. Evolution of Intrinsic and Extrinsic Electron Traps at Grain Boundary during Sintering ZnO Based Varistor Ceramics. *Materials* **2022**, *15*, 1098. [CrossRef] [PubMed]
12. Saboor, A.; Shah, S.M.; Hussain, H. Band gap tuning and applications of ZnO nanorods in hybrid solar cell: Ag-doped verses Nd-doped ZnO nanorods. *Mater. Sci. Semicond. Process.* **2019**, *93*, 215–225. [CrossRef]
13. Mishra, Y.K.; Adelung, R. ZnO tetrapod materials for functional applications. *Mater. Today* **2018**, *21*, 631–651. [CrossRef]

14. Qiu, Y.; Chen, W.; Yang, S. Facile hydrothermal preparation of hierarchically assembled, porous single-crystalline ZnO nanoplates and their application in dye-sensitized solar cells. *J. Mater. Chem.* **2010**, *20*, 1001–1006. [CrossRef]
15. Akhmedov, A.; Abduev, A.; Murliev, E.; Asvarov, A.; Muslimov, A.; Kanevsky, V. The ZnO-In_2O_3 Oxide System as a Material for Low-Temperature Deposition of Transparent Electrodes. *Materials* **2021**, *14*, 6859. [CrossRef] [PubMed]
16. Qiao, Z.; Xia, C.; Cai, Y.; Afzal, M.; Wang, H.; Qiao, J.; Zhu, B. Electrochemical and electrical properties of doped CeO_2-ZnO composite for low-temperature solid oxide fuel cell applications. *J. Power Sources* **2018**, *392*, 33–40. [CrossRef]
17. Pearton, S.; Norton, D.; Ip, K.; Heo, Y.; Steiner, T. Recent progress in processing and properties of ZnO. *Superlattices Microstruct.* **2003**, *34*, 3–32. [CrossRef]
18. Nava, O.; Soto-Robles, C.; Gómez-Gutiérrez, C.; Vilchis-Nestor, A.; Castro-Beltrán, A.; Olivas, A.; Luque, P. Fruit peel extract mediated green synthesis of zinc oxide nanoparticles. *J. Mol. Struct.* **2017**, *1147*, 1–6. [CrossRef]
19. Zeng, Q.-R.; Feng, J.-T.; Lin, X.-C.; Zhao, Y.; Liu, H.; Wang, S.-Z.; Dong, Z.-J.; Feng, W. One-step facile synthesis of a NiO/ZnO biomorphic nanocomposite using a poplar tree leaf template to generate an enhanced gas sensing platform to detect n-butanol. *J. Alloys Compd.* **2020**, *815*, 150550. [CrossRef]
20. Yang, Y.; Wang, X.; Yi, G.; Li, H.; Shi, C.; Sun, G.; Zhang, Z. Hydrothermal Synthesis of Co_3O_4/ZnO Hybrid Nanoparticles for Triethylamine Detection. *Nanomaterials* **2019**, *9*, 1599. [CrossRef] [PubMed]
21. Wang, Y.; Hao, X.; Wang, Z.; Dong, M.; Cui, L. Facile fabrication of $Mn2^+$ -doped ZnO photocatalysts by electrospinning. *R. Soc. Open Sci.* **2020**, *7*, 191050. [CrossRef] [PubMed]
22. Toe, M.Z.; Pung, S.-Y.; Le, A.T.; Yaccob, K.A.B.; Matsuda, A.; Tan, W.K.; Han, S.S. Morphology and optical properties of ZnO nanorods coupled with metal oxides of various bandgaps by photo-oxidation. *J. Lumin.* **2021**, *229*, 117649. [CrossRef]
23. Kaenphakdee, S.; Putthithanas, P.; Yodyingyong, S.; Leelawattanachai, J.; Triampo, W.; Sanpo, N.; Jitputti, J.; Triampo, D. Zinc Oxide Synthesis from Extreme Ratios of Zinc Acetate and Zinc Nitrate: Synergistic Morphology. *Materials* **2022**, *15*, 570. [CrossRef] [PubMed]
24. Youcef, R.; Benhadji, A.; Zerrouki, D.; Fakhakh, N.; Djelal, H.; Ahmed, M.T. Electrochemical synthesis of CuO–ZnO for enhanced the degradation of Brilliant Blue (FCF) by sono-photocatalysis and sonocatalysis: Kinetic and optimization study. *React. Kinet. Mech. Catal.* **2021**, *133*, 541–561. [CrossRef]
25. Krishnakumar, B.; Alsalme, A.; Alharthi, F.A.; Mani, D.; Anandan, K.; Amutha, P.; Sobral, A.J. Synthesis, characterization of gelatin assisted ZnO and its effective utilization of toxic azo dye degradation under direct sunlight. *Opt. Mater.* **2021**, *113*, 110854. [CrossRef]
26. Thatikayala, D.; Min, B. Ginkgo leaves extract-assisted synthesis of ZnO/CuO nanocrystals for efficient UV-induced photodegradation of organic dyes and antibacterial activity. *J. Mater. Sci. Mater. Electron.* **2021**, *32*, 17154–17169. [CrossRef]
27. Hua, J. Synthesis and characterization of gold nanoparticles (AuNPs) and ZnO decorated zirconia as a potential adsorbent for enhanced arsenic removal from aqueous solution. *J. Mol. Struct.* **2020**, *1228*, 129482. [CrossRef]
28. Cao, Y.; Dhahad, H.A.; El-Shorbagy, M.A.; Alijani, H.Q.; Zakeri, M.; Heydari, A.; Bahonar, E.; Slouf, M.; Khatami, M.; Naderifar, M.; et al. Dehkordi, Green synthesis of bimetallic ZnO-CuO nanoparticles and their cytotoxicity properties. *Sci. Rep.* **2021**, *11*, 23479. [CrossRef]
29. Kumar, C.R.R.; Betageri, V.S.; Nagaraju, G.; Pujar, G.H.; Onkarappa, H.S.; Latha, M.S. One-pot green synthesis of ZnO–CuO nanocomposite and their enhanced photocatalytic and antibacterial activity. *Adv. Nat. Sci. Nanosci. Nanotechnol.* **2020**, *11*, 015009. [CrossRef]
30. Muthukrishnaraj, A.; Kalaivani, S.S.; Manikandan, A.; Kavitha, H.P.; Srinivasan, R.; Balasubramanian, N. Sonochemical synthesis and visible light induced photocatalytic property of reduced graphene oxide@ZnO hexagonal hollow rod nanocomposite. *J. Alloys Compd.* **2020**, *836*, 155377. [CrossRef]
31. Arun, V.; Prabhu, S.; Priyadharsan, A.; Maadeswaran, P.; Sohila, S.; Ramesh, R.; Kumar, A.S. Facile, low cost synthesis of cauliflower-shaped ZnO with MWCNT/rGO nanocomposites and their photocatalytic activity. *J. Mater. Sci. Mater. Electron.* **2021**, *32*, 15763–15777. [CrossRef]
32. Nundy, S.; Eom, T.-Y.; Song, K.-Y.; Park, J.-S.; Lee, H.-J. Hydrothermal synthesis of mesoporous ZnO microspheres as NOX gas sensor materials—Calcination effects on microstructure and sensing performance. *Ceram. Int.* **2020**, *46*, 19354–19364. [CrossRef]
33. Rambabu, K.; Bharath, G.; Banat, F.; Show, P.L. Green synthesis of zinc oxide nanoparticles using Phoenix dactylifera waste as bioreductant for effective dye degradation and antibacterial performance in wastewater treatment. *J. Hazard. Mater.* **2020**, *402*, 123560. [CrossRef]
34. Rahman, A.; Harunsani, M.H.; Tan, A.L.; Khan, M.M. Zinc oxide and zinc oxide-based nanostructures: Biogenic and phytogenic synthesis, properties and applications. *Bioprocess Biosyst. Eng.* **2021**, *44*, 1333–1372. [CrossRef] [PubMed]
35. Mohamed, R.M.; Ismail, A.A. Photocatalytic reduction and removal of mercury ions over mesoporous CuO/ZnO S-scheme heterojunction photocatalyst. *Ceram. Int.* **2021**, *47*, 9659–9667. [CrossRef]
36. Prajapati, A.K.; Mondal, M.K. Novel green strategy for CuO–ZnO–C nanocomposites fabrication using marigold (*Tagetes* spp.) flower petals extract with and without CTAB treatment for adsorption of Cr(VI) and Congo red dye. *J. Environ. Manag.* **2021**, *290*, 112615. [CrossRef] [PubMed]
37. Khan, M.A.; Nayan, N.; Ahmad, M.K.; Fhong, S.C.; Ali, M.S.M.; Mustafa, M.K.; Tahir, M. Interface study of hybrid CuO nanoparticles embedded ZnO nanowires heterojunction synthesized by controlled vapor deposition approach for optoelectronic devices. *Opt. Mater.* **2021**, *117*, 111132. [CrossRef]

38. Saratale, R.G.; Saratale, G.D.; Cho, S.-K.; Ghodake, G.; Kadam, A.; Kumar, S.; Mulla, S.I.; Kim, D.-S.; Jeon, B.-H.; Chang, J.S.; et al. Phyto-fabrication of silver nanoparticles by *Acacia nilotica* leaves: Investigating their antineoplastic, free radical scavenging potential and application in H_2O_2 sensing. *J. Taiwan Inst. Chem. Eng.* **2019**, *99*, 239–249. [CrossRef]
39. Rather, L.J.; Islam, S.-U.; Mohammad, F. *Acacia nilotica* (L.): A review of its traditional uses, phytochemistry, and pharmacology. *Sustain. Chem. Pharm.* **2015**, *2*, 12–30. [CrossRef]
40. Ramesh, S.; Vinitha, U.; Anthony, S.P.; Muthuraman, M.S. Pods of *Acacia nilotica* mediated synthesis of copper oxide nanoparticles and it's in vitro biological applications. *Mater. Today Proc.* **2021**, *47*, 751–756. [CrossRef]
41. Rao, T.N.; Babji, P.; Ahmad, N.; Khan, R.A.; Hassan, I.; Shahzad, S.A.; Husain, F.M. Green synthesis and structural classification of *Acacia nilotica* mediated-silver doped titanium oxide (Ag/TiO_2) spherical nanoparticles: Assessment of its antimicrobial and anticancer activity. *Saudi J. Biol. Sci.* **2019**, *26*, 1385–1391. [CrossRef] [PubMed]
42. Da'Na, E.; Taha, A.; Afkar, E. Green Synthesis of Iron Nanoparticles by *Acacia nilotica* Pods Extract and Its Catalytic, Adsorption, and Antibacterial Activities. *Appl. Sci.* **2018**, *8*, 1922. [CrossRef]
43. Sakhaei, Z.; Rezaei, M. Mechanochemical synthesis of $ZnO.Al_2O_3$ powders with various Zn/Al molar ratios and their applications in reverse water-gas shift reaction. *Environ. Sci. Pollut. Res.* **2021**, *28*, 13790–13799. [CrossRef] [PubMed]
44. Gajendiran, J.; Rajendran, V. Synthesis and characterization of coupled semiconductor metal oxide (ZnO/CuO) nanocomposite. *Mater. Lett.* **2014**, *116*, 311–313. [CrossRef]
45. Kampara, R.K.; Sonia, T.; Jeyaprakash, B.G. CuO/ZnO Heterojunction Nanograins: Methanol Vapour Detection. *J. Electron. Mater.* **2021**, *50*, 2482–2495. [CrossRef]
46. Mali, S.M.; Narwade, S.S.; Navale, Y.H.; Tayade, S.B.; Digraskar, R.V.; Patil, V.B.; Kumbhar, A.S.; Sathe, B.R. Heterostructural CuO-ZnO Nanocomposites: A Highly Selective Chemical and Electrochemical NO_2 Sensor. *ACS Omega* **2019**, *4*, 20129–20141. [CrossRef] [PubMed]
47. Lavín, A.; Sivasamy, R.; Mosquera, E.; Morel, M.J. High proportion ZnO/CuO nanocomposites: Synthesis, structural and optical properties, and their photocatalytic behavior. *Surfaces Interfaces* **2019**, *17*, 100367. [CrossRef]
48. Wilson, D.A.; Gurung, K.; Langell, M.A. Effect of zinc substitution on the growth morphology of ZnO-CuO tenorite solid solutions. *J. Cryst. Growth* **2021**, *562*, 126062. [CrossRef]
49. Yakout, S.M.; El-Sayed, A.M. Enhanced ferromagnetic and photocatalytic properties in Mn or Fe doped p-CuO/n-ZnO nanocomposites. *Adv. Powder Technol.* **2019**, *30*, 2841–2850. [CrossRef]
50. Kumari, V.; Yadav, S.; Jindal, J.; Sharma, S.; Kumari, K.; Kumar, N. Synthesis and characterization of heterogeneous ZnO/CuO hierarchical nanostructures for photocatalytic degradation of organic pollutant. *Adv. Powder Technol.* **2020**, *31*, 2658–2668. [CrossRef]
51. Mansournia, M.; Ghaderi, L. CuO@ZnO core-shell nanocomposites: Novel hydrothermal synthesis and enhancement in photocatalytic property. *J. Alloys Compd.* **2017**, *691*, 171–177. [CrossRef]
52. Hessien, M.; Da'Na, E.; Al-Amer, K.; Khalaf, M.M.; D'Na, E. Nano ZnO (hexagonal wurtzite) of different shapes under various conditions: Fabrication and characterization. *Mater. Res. Express* **2019**, *6*, 085057. [CrossRef]
53. Quirino, M.R.; Lucena, G.L.; Medeiros, J.A.; dos Santos, I.M.G.; De Oliveira, M.J.C. CuO Rapid Synthesis with Different Morphologies by the Microwave Hydrothermal Method. *Mater. Res.* **2018**, *21*, e20180227. [CrossRef]
54. Gao, P.; Liu, D. Facile synthesis of copper oxide nanostructures and their application in non-enzymatic hydrogen peroxide sensing. *Sens. Actuators B Chem.* **2015**, *208*, 346–354. [CrossRef]
55. Chen, H.; Shin, D.-W.; Lee, J.-H.; Park, S.-M.; Kwon, K.-W.; Yoo, J.-B. Three-dimensional CuO nanobundles consisted of nanorods: Hydrothermal synthesis, characterization, and formation mechanism. *J. Nanosci. Nanotechnol.* **2010**, *10*, 5121–5128. [CrossRef] [PubMed]
56. Ullah, H.; Mushtaq, L.; Ullah, Z.; Fazal, A.; Khan, A.M. Effect of vegetable waste extract on microstructure, morphology, and photocatalytic efficiency of ZnO–CuO nanocomposites. *Inorg. Nano-Metal Chem.* **2021**, *51*, 963–975. [CrossRef]
57. Kumari, V.; Sharma, S.; Sharma, A.; Kumari, K.; Kumar, N. Hydrothermal synthesis conditions effect on hierarchical ZnO/CuO hybrid materials and their photocatalytic activity. *J. Mater. Sci. Mater. Electron.* **2021**, *32*, 9596–9610. [CrossRef]
58. Lu, P.; Zhou, W.; Li, Y.; Wang, J.; Wu, P. Abnormal room temperature ferromagnetism in CuO/ZnO nanocomposites via hydrothermal method. *Appl. Surf. Sci.* **2017**, *399*, 396–402. [CrossRef]
59. Chang, T.; Li, Z.; Yun, G.; Jia, Y.; Yang, H. Enhanced Photocatalytic Activity of ZnO/CuO Nanocomposites Synthesized by Hydrothermal Method. *Nano-Micro Lett.* **2013**, *5*, 163–168. [CrossRef]
60. Bordbar, M.; Negahdar, N.; Nasrollahzadeh, M. *Melissa officinalis* L. leaf extract assisted green synthesis of CuO/ZnO nanocomposite for the reduction of 4-nitrophenol and Rhodamine B. *Sep. Purif. Technol.* **2018**, *191*, 295–300. [CrossRef]